COBEM 2021 26th International Congress of Mechanical Engineering
ABCM Associação Brasileira de Engenharia e Ciências Mecânicas
November 22-26, 2021, Virtual Congress, Brazil

COB-2021-0030 THERMODYNAMIC MODELING OF A TWO-STAGE REFRIGERATION SYSTEM FOR A BATTERY ELECTRIC VEHICLE

George Luiz Rincaweski Vegini
Guilherme Borges Ribeiro
Aeronautics Institute of Technology, Praça Marechal Eduardo Gomes, São José dos Campos, Brazil
georgev@ita.br
gbribeiro@ita.br

Abstract. *Following the market and environmental concerns, the development and commercialization of hybrid powertrain and battery electric vehicles (BEV) increased in the last years. With the consistent increase of energy storage, an efficient and compact scheme of battery thermal management systems is a crucial aspect that must be taken into account for an adequate BEV operation. The most common technologies used are air cooling, liquid cooling, heat pipes, or direct refrigerant cooling. Focusing on the latter type, a vapor-compression refrigeration system can be used to extract the battery heat and provide cabin temperature comfort through two distinct evaporators connected to the same compressor. The performance of the two-stage refrigeration cycle is a key aspect to ensure a proper vehicle range without overloading the electrical grid. Also, the battery surface temperature must be kept below pre-defined values to avoid battery runaway and reduction of lifespan. Moreover, the use of environmental-friendly refrigerant fluids is also envisaged to reduce the global warming impact and CO2 emissions in future BEV. Considering all these aspects, this paper proposes an endoreversible thermodynamic modeling of a two-stage refrigeration system responsible for the battery and cabin cooling that makes use of R-134a as refrigerant fluid. The battery and cabin heat generation are considered as data input for the proposed modeling. A positive displacement compressor with fixed volumetric and global efficiencies is modeled, and constant global thermal conductances are considered for both evaporators and condenser. The heat exchangers were discretized in zones related to the fluid phase. The final system condition was achieved numerically using the software Engineering Equation Solver (EES). The distribution of the total global thermal conductance between heat exchangers is evaluated as a manner to align good performance and system compactness. The performance comparison with different refrigerants as R-1234ze, R-1234yf, and R-32 is part of the analysis. Results can serve as guidelines for the future design of hybrid powertrains and BEV.*

Keywords: *Refrigeration, modeling, battery cooling, electric vehicle, refrigerant fluid*

1. INTRODUCTION

Transport is a significant source of greenhouse gases emissions. In the European union, emissions from passenger cars and vans represent 15% of the total greenhouse emissions, as of 2018 (Buysse and Miller, 2021). Thus, following environmental concerns, there has been a transition in the automotive market from internal combustion to electric vehicles. From 2013 to 2018 there has been a 14 times increase in battery electric vehicle (BEV) deployment in the world (IEA, 2019).

There are several configurations for electric vehicles, among them, hybrid, plug-in and battery. BEV are the most common, being the Li-ion battery the most used. However, Li-ion battery is very sensitive to temperature for its functioning, as operating outside its ideal ranges can cause thermal runaway and reduces drastically the battery power and life cycle (Wickramaratne, 2017). Therefore, an efficient and compact scheme of battery thermal management system is a crucial aspect that must be taken into account when designing such vehicles. The most common technologies for battery thermal management are air cooling, liquid cooling, heat pipes, or direct refrigerant cooling (Kim *et al.*, 2019). Focusing on the latter type, a vapor-compression refrigeration system can be used to extract the battery heat and provide cabin temperature comfort through two distinct evaporators connected to the same compressor, such structure is called a two-stage refrigeration system. The idea of this paper is to mathematically model this system and evaluate how its core parameters affects its performance.

There is yet another issue to be considered, most of the refrigerant fluids used are hydrofluorocarbons, some of which also have a high potential for global warming. R-134a, which is the most used has a high potential. There are, however, alternatives to be considered, some of them are R-1234yf, R-1234ze(E) and R-32 (Pham and Rajendran, 2012). This paper will also compare the performance of these different refrigerant fluids for the proposed system.

2. MODEL DESCRIPTION

The model proposed for the BEV thermal management is that of a vapor compression system that cools simultaneously the cabin and the battery using the same compressor, hence, a two-stage configuration.

This paper will approach the model with a thermodynamic endoreversilble analysis. The devices are considered with constant global thermal conductance for the heat transfer study.

In the proposed system, the cabin environment is refrigerated and its humidity controlled with an evaporator, as already occurs in internal combustion vehicles. The battery has its heat generated dissipated by an evaporator by direct refrigerant cooling.

It is known that both the cabin and the battery have variable heat generation throughout the vehicle service, for example, during battery charging and fast discharge (acceleration) the battery is main source of heat for the system. Meanwhile, during a hot day with constant driving, the cabin demands more of the thermal management system. Therefore, the refrigeration system must be able to answer properly to these different configurations. The amount of heat needed to be removed from the cabin and the battery are considered as data input, as these are the parameters that rule the system.

The two-stage model for the refrigeration of a battery vehicle is shown in Fig. 1. This model has the advantages of allowing the evaporators to operate at different mass flow rates and pressures, responding accordingly to the demands of the cabin and the battery.

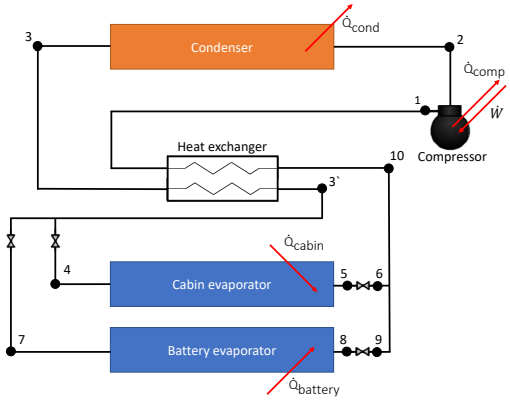

Figure 1. Two-stage model for the refrigeration of a battery vehicle.

It is chosen to add a heat exchanger to the model and evaluate its impact on the system. Such type of heat exchanger is common in similar situations, like cabin control for internal combustion vehicles and domestic refrigerators. Condenser and evaporators are discretized into zones related to the fluid phase and have no change in pressure. Psychrometry is considered in the cabin evaporator. The fluid pipes are simplified, with no change in pressure and no heat exchange with the environment. To avoid liquid phase in the compressor chamber there is a superheating temperature, ΔT_{sup}, in both evaporators. To avoid mass flow instability it is applied a cooling temperature, ΔT_{sub} , in the condenser.

It is also calculated the losses of the system by mensuring the entropy generation of each device. The second law analysis from this section, except for the heat exchanger, has as reference Bahman and Groll (2020). The entropy generated at the system is the sum of the entropies generated by each device.

2.1 Compressor

It is considered a generic positive displacement compressor, as it is commonly used in the automotive industry. The compressor global efficiency, η_G, is described by Eq. (1) and its volumetric efficiency, η_V, by Eq. (2).

$$\eta_G = \frac{\dot{m}(h_{2s} - h_1)}{\dot{W}}, \tag{1}$$

$$\eta_V = \frac{\dot{m}}{\frac{V}{v_1} rot}, \tag{2}$$

where $\dot{m}$, $\dot{W}$, rot, V, v and h represents the mass flow of the system, compressor power, compressor rotation, volume displaced, specific volume and specific enthalpy, respectively. The indexes inform the state that the property is evaluated. The index s represents a isentropic process.

From the first law of thermodynamics one can deduce:

$$\dot{Q}_{comp} + \dot{W} = \dot{m}(h_2 - h_1), \tag{3}$$

where $\dot{Q}_{comp}$ is the heat transfer rate of the compressor. This heat transfer can be calculated by knowing the thermal conductance of the compressor, UA_{comp}, as,

$$\dot{Q}_{comp} = UA_{comp}(T_{out} - T_2), \tag{4}$$

where T_2 and T_{out} are the temperatures at the the exhaust of the compressor and at the outdoor, respectively. From previous knowledge it is considered that the compressor is at the temperature of its exhaust and UA_{comp} is close to zero.

The compressor displacement volume is an input parameter, however, when comparing different refrigerant fluids it is not fair to use the same volume, as the fluids have different specific volumes and enthalpies. For adequate comparisons, the authors choose one compressor displacement volume for R134a as standard and update the value for each other fluid using a relation based on the volumetric refrigerant effect, VRE, as shown in the Eq. (5).

$$V = V_{R134a}\frac{VRE_{R134a}}{VRE} \tag{5}$$

The volumetric refrigerant effect is the ratio between the enthalpy of vaporization and the specific volume at a determined temperature. It is chosen 15°C as the evaluation temperature.

The entropy generated by the compressor, $\dot{S}_{comp}$, is

$$\dot{S}_{comp} = \dot{m}(s_2 - s_1) - \frac{\dot{Q}_{comp}}{T_{out}}, \tag{6}$$

where s represents specific entropy.

2.2 Condenser

The condenser rejects heat from the cycle into the atmosphere, therefore, it is ruled by the difference of temperatures between the condenser and the outdoor, being the latter considered constant. It is important to remember that the thermal conductance needed to achieve the heat transfer desired is dependent of external variables like vehicle speed and fan size. These type of parameters are not considered in this work, as the objective is to quantify how much the thermal conductance must be for the system to work properly at determined condition, and not how to achieve it.

The condenser is discretized into three zones, each zone related to the fluid phase: subheated, two-phase and superheated. The total heat transfered by the condenser, $\dot{Q}_{cond}$, is the sum of the heat transfer rate of each zone. Similarly, the thermal conductance of the condenser is the sum of the thermal conductance of each individual zones.

Applying the first law of thermodynamics on each zone one obtains:

$$\dot{Q}_{cond,sh} = \dot{m}(h_{cond,v} - h_2), \tag{7}$$

$$\dot{Q}_{cond,tp} = \dot{m}(h_{cond,l} - h_{cond,v}), \tag{8}$$

$$\dot{Q}_{cond,sub} = \dot{m}(h_3 - h_{cond,l}), \tag{9}$$

where the indexes v and l indicates that the properties are evaluated at the saturated vapor and saturated liquid states, respectively.

Each zone needs to be analysed individually to determine its thermal conductance. Using the effectiveness-number of tranfers units (NTU) from Incropera *et al.* (2006) one obtains:

$$\dot{Q}_{cond,sh} = -\dot{m}c_{p,cond}\Delta T_{cond}\left[1 - \mathbf{exp}\left(-\frac{UA_{cond,sh}}{\dot{m}c_{p,cond}}\right)\right]; \tag{10}$$

$$\dot{Q}_{cond,tp} = -UA_{cond,tp}\Delta T_{cond}; \tag{11}$$

$$\dot{Q}_{cond,sub} = -\dot{m}c_{p,3}\Delta T_{cond}\left[1 - \mathbf{exp}\left(-\frac{UA_{cond,sub}}{\dot{m}c_{p,3}}\right)\right]. \tag{12}$$

The entropy generated by the condenser, $\dot{S}_{cond}$, is

$$\dot{S}_{gen,cond} = \dot{m}(s_3 - s_2) - \frac{\dot{Q}_{cond}}{T_{out}}. \tag{13}$$

2.3 Cycle heat exchanger

The heat exchanger efficiency equation is (Musser *et al.*, 2016):

$$\eta_{hx} = \frac{h_1 - h_{10}}{h(P_1; T_3) - h_{10}}. \tag{14}$$

With the addition of the heat exchanger, the system demands a new equation for closure. This new equation is deduced applying the first law of thermodynamics at the heat exchanger.

$$h_3 - h_{3'} + h_{10} - h_1 = 0 \tag{15}$$

The entropy generated by the heat exchanger is calculated as,

$$\dot{S}_{gen,hx} = \frac{\dot{m}}{T_{out}}(\psi_3 - \psi_{3'} + \psi_{10} - \psi_1), \tag{16}$$

where ψ represents specific exergy (availability).

2.4 Cabin evaporator

The cabin evaporator withdraws heat and humidity from the cabin. Similarly to the condenser, the model for the evaporators is also discretized into zones accordingly to the refrigerant fluid phase, however, for the evaporators there is no subheated phase. The total heat transferred by the evaporator, $\dot{Q}_{cab}$, is the sum of the heat transfer rate of each zone. The thermal conductance of the evaporator is the sum of the thermal conductance of each individual zones.

Applying the first law of thermodynamics on the two-phase zone one obtains:

$$\dot{Q}_{cab,tp} = \dot{m}_{cab}(h_{cab,v} - h_4). \tag{17}$$

From psychrometry, the heat transferred by the two-phase zone is equal to the sum of the sensible and latent portions. Each portion is calculated as:

$$\dot{Q}_{cab,tp,sen} = UA_{cab,tp,sen}\Delta T_{cab} \tag{18}$$

$$\dot{Q}_{cab,tp,lat} = UA_{cab,tp,lat}(\omega_{in} - \omega_{cab})h_{lv,tp} \tag{19}$$

where ω and h_{lv} indicate absolute humidity and specific enthalpy of vaporization of water, respectively. The value of ω_{cab} is evaluated for relative humidity of one at the evaporator temperature. It is important to remember that $UA_{cab,tp,lat}$ in Eq. 19 is not thermal conductance, but mass conductance. Mass and thermal conductances are linked by the Lewis number relation (Simões-Moreira and Neto, 2019), as shown in Eq. 20.

$$R_{Le} = \frac{UA_{cab,tp,sen}}{UA_{cab,tp,lat}c_{p,in}} \tag{20}$$

As humidity is withdrawn from the cabin and this process cannot occur the other way around, if $\omega_{in} < \omega_{cab}$, there is no latent heat transferred, which means that $\dot{Q}_{cab,tp,lat}$ and $UA_{cab,tp,lat}$ are both zero.

Similarly to the two-phase model, the equations for the superheated model are:

$$\dot{Q}_{cab,sh} = \dot{m}_{cab}(h_5 - h_{cab,v}) \tag{21}$$

$$\dot{Q}_{cab,sh,sen} = \dot{m}_{cab}c_{p,cab}\Delta T_{cab}\left[1 - \mathbf{exp}\left(-\frac{UA_{cab,sh,sen}}{\dot{m}_{cab}c_{p,cab}}\right)\right] \tag{22}$$

$$\dot{Q}_{cab,sh,lat} = UA_{cab,sh,lat}(\omega_{in} - \omega_{cab,sh})h_{lv,sh} \tag{23}$$

$$R_{Le} = \frac{UA_{cab,sh,sen}}{UA_{cab,sh,lat}c_{p,in}} \tag{24}$$

The exact same psychrometric analysis occurs for this zone, such so, that if $\omega_{in} < \omega_{cab,sh}$, there is no latent heat transferred, which means that $\dot{Q}_{cab,sh,lat}$ and $UA_{cab,sh,lat}$ are both zero.

The entropy generated by the cabin evaporator, $\dot{S}_{gen,c}$ is

$$\dot{S}_{gen,cab} = \dot{m}_{cab}(s_5 - s_4) - \frac{\dot{Q}_{cab}}{T_{in}} \tag{25}$$

2.5 Battery evaporator

The battery evaporator extracts heat directly from the battery, therefore, the model for this evaporator is exactly the same as the previous one without the psychrometrics considerations. Therefore, the equations are:

$$\dot{Q}_{bat,tp} = \dot{m}_{bat}(h_{bat,v} - h_4) \tag{26}$$

$$\dot{Q}_{bat,sh} = \dot{m}_{bat}(h_5 - h_{bat,v}) \tag{27}$$

$$\dot{Q}_{bat,tp} = UA_{bat,tp}\Delta T_{bat} \tag{28}$$

$$\dot{Q}_{bat,sh} = \dot{m}_{bat}c_{p,bat}\Delta T_{bat}\left[1 - \mathbf{exp}\left(-\frac{UA_{bat,sh}}{\dot{m}_{bat}c_{p,bat}}\right)\right] \tag{29}$$

The entropy generated by the battery evaporator, $\dot{S}_{gen,bat}$ is

$$\dot{S}_{gen,bat} = \dot{m}_{bat}(s_8 - s_7) - \frac{\dot{Q}_{bat}}{T_{bat}} \tag{30}$$

In this model the authors consider that the battery temperature is homogeneous.

For closure the model of the system still needs a few equations, which are mass conservation (Eq. 31) and energy conservation (Eq. 32).

$$\dot{m} = \dot{m}_{cab} + \dot{m}_{bat} \tag{31}$$

$$\dot{m}h_{10} = \dot{m}_{cab}h_6 + \dot{m}_{bat}h_9 \tag{32}$$

2.6 Expansion valves

The process that occurs at the expansion valves is considered isenthalpic, but not isentropic. The entropy generated at each expansion valve, $\dot{S}_{gen,exv}$, is

$$\dot{S}_{gen,exv} = \dot{m}(s_{outlet} - s_{inlet}). \tag{33}$$

3. SETTING

The model was implemented and solved using the software Engineering Equation Solver - EES (Klein, 2016). The model is very sensitive to the guesses of the first iteration, to stipulate such guesses, the exact same model was firstly solved for simple situations using an algorithm developed by the authors in python using successive substitution method.

Table 1 shows the input parameters for the model. Most of these parameters are representative for similar models and were chosen by the authors from previous knowledge. The heat needed to be withdrawn from the cabin, $\dot{Q}_{cab}$, particularly, was chosen from dos Santos (2005).

The stop criteria used is the standard suggestion from EES, 1.10^{-6}, for the relative residuals.

4. RESULTS AND DISCUSSION

Firstly, the model was solved so that ΔT_{cond},ΔT_{cab} and ΔT_{bat} were 10°C, 10°C and 20°C, respectively. Table 2 shows these results. The thermal conductances from this scenario will be considered, henceforth, the standard.

One can observe from Tab. 2 that the results for R-32 differentiate the most from the average, particularly for the pressures. Its coefficient of performance is by far the worst. As it will be seen, R-32 will have the most distinct results in every scenario.

The thermal conductance for the battery is very inferior when compared to the condenser and the cabin. That is natural, as the heat generated by the battery in this scenario is also very inferior to the the heat transfer in the cabin and the condenser.

4.1 System heat exchanger analysis

It was analysed the impact of the heat exchanger in the system for the standard scenario (thermal conductances from Tab. 2). Figure 2 shows how the coefficient of performance responds to the variation of the heat exchanger efficiency for each refrigerant fluid, where η_{hx} equal to zero is no heat exchanger at all, and equal to 1.0 is the perfect heat exchanger with infinite surface.

The insertion of a perfect heat exchanger improves the system of R-134a, R-1234ze, R-1234yf and R-32 by 5,65%, 9,92%, 7,43% and 0,61%, respectively. Here, again, the deviancy is the system with R-32, which shows almost no improvement.

Table 1. Input parameters

Parameter	Value	Unit
V_{R134a}	27.10^{-6}	m^3
η_G	0.6	-
η_V	0.7	-
η_{hx}	0.9	-
T_{cab}	27.0	°C
Φ_{cab}	0.5	-
T_{out}	35.0	°C
T_{bat}	30.0	°C
P_{atm}	1.0	atm
R_{Le}	1.0	-
ΔT_{sup}	5.0	°C
ΔT_{sub}	5.0	°C
UA_{comp}	0.5	W/K
$\dot{Q}_{cab}$	5.0	kW
$\dot{Q}_{bat}$	2.0	kW

Table 2. Results for the standard scenario.

	R-134a	R-1234ze	R-1234yf	R-32	Unit
COP	4.24	4.35	4.24	3.81	-
$\dot{S}_{gen}$	4.82	4.68	4.82	5.43	W/K
$\dot{m}$	0.0403	0.0433	0.0493	0.0255	kg/s
rot	120.4	120.6	120.6	121.8	rps
$\dot{W}$	1.65	1.61	1.65	1.84	kW
P_{cond}	11.61	8.77	11.54	27.95	bar
P_{cab}	5.21	3.90	5.42	13.56	bar
P_{bat}	4.15	3.10	4.38	11.07	bar
UA_{cond}	743.8	763.6	758.9	658.8	W/K
UA_{cab}	505.3	506.5	506.9	504.7	W/K
UA_{bat}	100.4	100.5	100.5	100.3	W/K

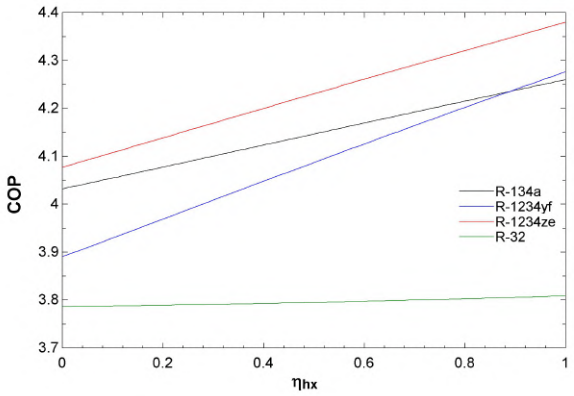

Figure 2. Heat exchanger influence in the system.

4.2 Heat demand

It was analyzed how the system responds to different heat demands from the cabin and the battery, for the standard scenario (thermal conductances from Tab. 2). Figure 3 shows how the coefficient of performance of the system respond to the variation of the heat needed to be dissipated by the cabin. Figure 4 shows how the coefficient of performance of the system respond to the variation of the heat generated by the battery.

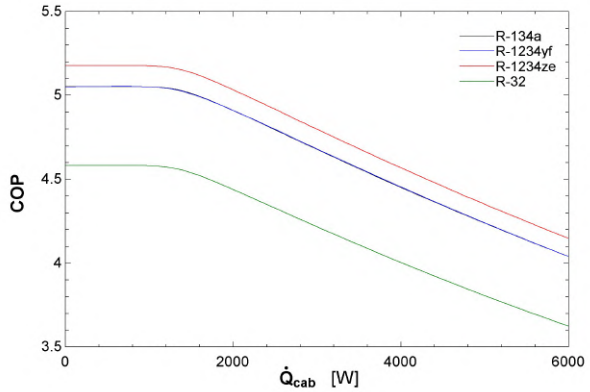

Figure 3. Influence of the heat from the cabin in the system. The results for R-134a and R-1234yf are equal.

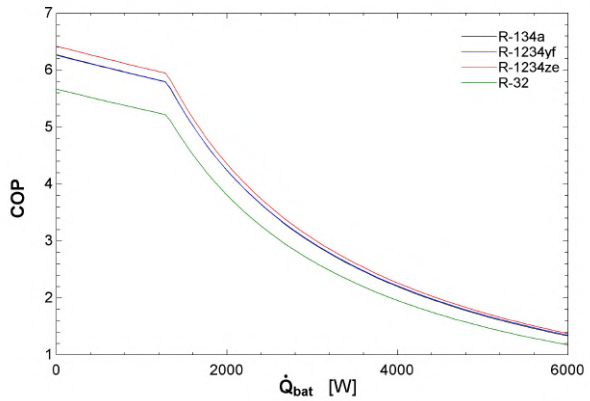

Figure 4. Influence of the heat generated by the battery in the system. The results for R-134a and R-1234yf are equal.

In both situations, for every refrigerant, there is an initial plateau and then there is a significant decrease in performance. What causes this difference is the evaporator pressure. In the cabin situation, the plateau appears as the evaporator pressure is initially constant, until it starts to drop, as the vaporization enthalpy at that pressure can no longer fulfill the demand from the cabin. In the battery situation the change comes as the pressure from the cabin evaporator surpasses the one from the battery evaporator.

Considering now that the total heat demand from the system, $\dot{Q}_{sum}$, is constant, one can evaluate how the heat from each source influences the system. Figure 5 shows the influence of the heat generated by the battery in the system for constant total heat demand of 7.0kW, for R-134a.

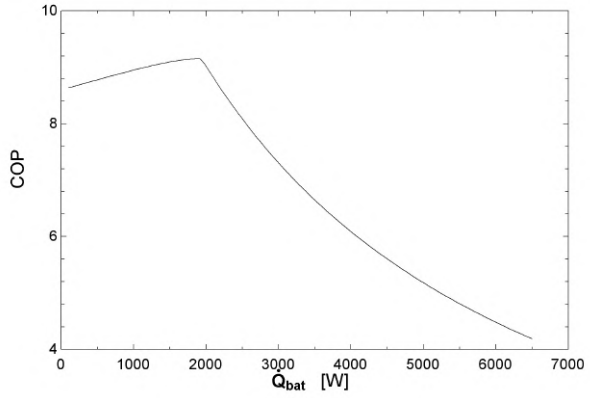

Figure 5. Influence of the heat generated by the battery in the system for constant total heat demand of 7.0kW, for R-134a.

There is a clear optimum, which is when the temperature from the cabin evaporator equals the battery evaporator. The same behaviour appears for other values of total heat demand and other fluids. Setting, then, the evaporators to the

same temperature and evaluating the total heat demand one obtains Fig. 6. This graph can be interpreted as a map for optimization of the system towards the total heat demand.

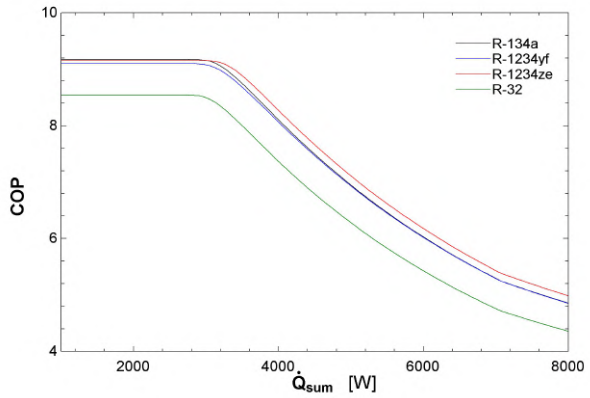

Figure 6. Heat demand optimazion map.

4.3 Thermal conductances

It was analysed the impact of the thermal conductances of the heat exchangers (condeser and evaporators) for the standard model. Figures 7,8 and 9 presents the influence of condeser, cabin evaporator and battery evaporator thermal conductance, respectively.

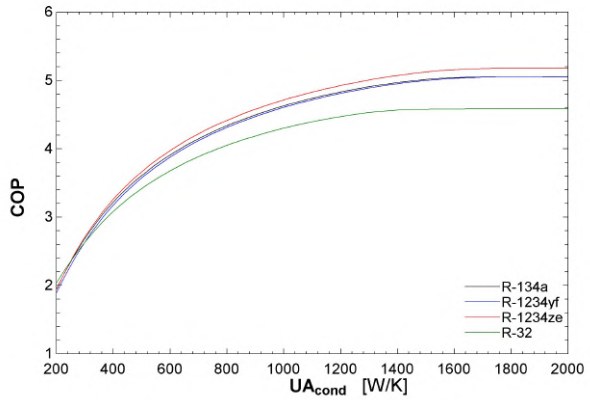

Figure 7. Influence of the condenser thermal conductance in the system.

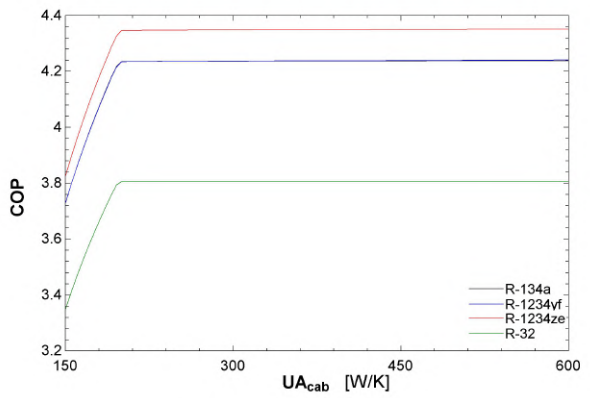

Figure 8. Influence of the cabin evaporator thermal conductance in the system. The results for R-134a and R-1234yf are equal.

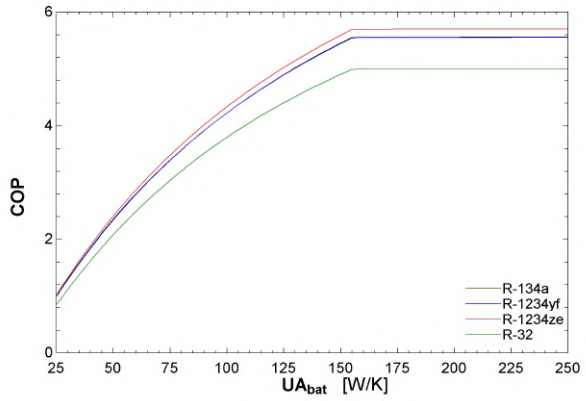

Figure 9. Influence of the battery evaporator thermal conductance in the system. The results for R-134a and R-1234yf are equal.

The evaporators have a quite bizarre influence in the system by achieving a peak performance and remaining constant at it no matter its thermal conductance increase. To understand this behaviour one must think at which evaporator is operating at a lower pressure. For example in the first moment in Fig. 8, the cabin evaporator is operating at a lower pressure. As soon as the battery evaporator has the lower pressure it achieves the plateau. The same happens for Fig. 9, except that in the first part the battery evaporator has the lower pressure.

Similarly to the heat demand situation, it is analysed how the components of thermal conductance affects a constant total thermal conductance, where, this total thermal conductance, UA_{sum}, is the sum of the condenser and cabin evaporator thermal conductances. Figure 10 presents the influence of the condenser thermal conductance for total thermal conductance of 1200W/K, for R-134a. There is a clear optimum, which is when the evaporators are at the same pressure. The same behaviours appears for other values of total thermal conductance and other fluids. Setting, then, the evaporators to the same pressure and evaluating the total thermal conductance one obtains Fig. 11. This graph can be interpreted as a map for optimization of the thermal conductance distribution of the system.

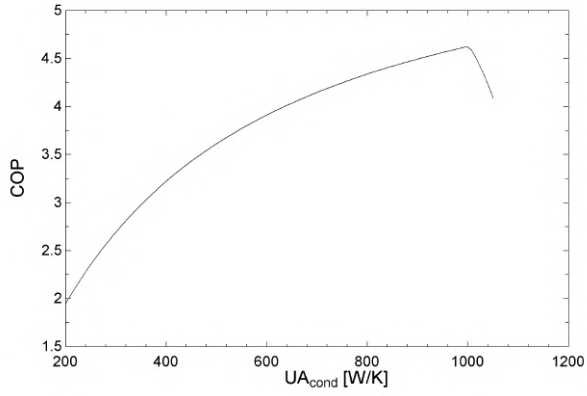

Figure 10. Influence of the condenser thermal conductance for total thermal conductance of 1200W/K, for R-134a.

4.4 Second law analysis

For the second law analysis it was calculated the entropy generation of each device for the standard scenario. Table 3 presents the percentage of entropy generated by each device towards the total.

The compressor generates the most entropy, followed by the condenser. The R-32, once again deviates from the others, having the condenser generating circa of 5% more entropy than in the others fluids. The cabin evaporator generates more entropy than the battery one, which is expected. It must be remembered that in this scenario, the heat from the cabin is 2.5 times greater than the heat from the battery. The expansion valves are the third biggest source of entropy. This is one big disadvantage from this model, as at any moment, for evaporators at different pressures, there are three expansion valves at operation, causing important loses to the system.

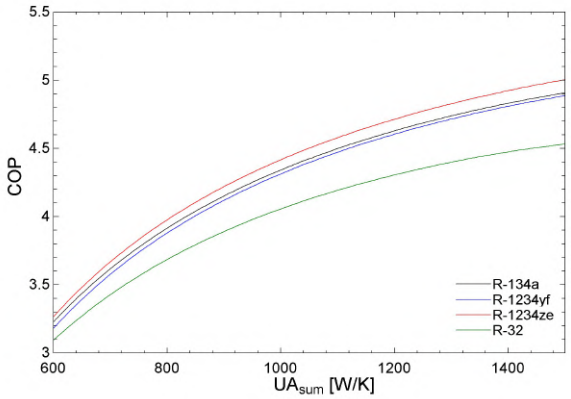

Figure 11. Thermal conductance optimization map.

Table 3. Percentage of entropy generated by each device for the standard scenario.

Device	**R-134a**	**R-1234ze**	**R-1234yf**	**R-32**
Compressor	38.82	39.56	39.65	35.78
Condenser	26.27	25.06	24.62	31.99
Heat exchanger	0.98	0.99	1.13	1.01
Cabin evaporator	11.80	12.02	11.81	10.50
Battery evaporator	9.62	9.83	9.63	8.56
Expansion valves	12.52	12.55	13.15	12.15

5. CONCLUSIONS

It was developed a computational model of a two-stage refrigeration system for a battery electric vehicle. The model consists of generic representative parameters that can be easily fitted into future designs of hybrid powertrains and BEV. Four refrigerant fluids were considered: R-134a, R-1234yf, R-1234ze and R-32. The latter showed the most deviancies from the average results.

It was calculated how the presence of a cycle heat exchanger (Fig. 2) affects the system. It was concluded that the presence of the heat exchanger can improve the coefficient of performance by up to approximately 10%. However, for R-32, there was no improvement at all.

It was evaluated how the heat sources, cabin and battery, affect the system. Figures 3 and 4 present the results for the mentioned. It was also considered a constant total heat demand (Fig. 5), and an optimum was achieved for evaporators operating at the same pressure. With this information it was generated a map for optimizing the system varying the values for the total heat sources, as shown in Fig. 6.

A similar analysis was made for the thermal conductances, evaluating how the system responds to different values of thermal conductance from the condenser (Fig. 7), cabin evaporator (Fig. 8) and battery evaporator (Fig. 9). A peak performance was achieved when considering a constant total thermal conductance that is the sum of the thermal conductances from the condenser and the cabin evaporator, as shown in Fig. 10. The peak performance is when the evaporators are at the same pressure. With this information it was generated a map for optimizing the system varying the values for the total thermal conductance (Fig. 11).

A second law analysis was made, by evaluating the loses from each device, taking the entropy generation into consideration, as shown in table 3. The compressor is the biggest source of entropy, representing up to approximately 40% of the total entropy generated by the system. The condenser is the second biggest source, followed by the expansion valves.

The absolute main conclusion for this paper is that this system, operating with two evaporators at different pressures, is less efficient than the same system, with two evaporators at the same pressure.

Figures 6 and 11 provide optimization maps for future projects involving thermal management of battery electric vehicles.

Validation and comparison of the obtained results with an experimental model is recommended. It is suggested to add more parameters to the system, like drop of pressure in the devices and heat exchange in the lines. It is encouraged to consider a more complete heat transfer analysis, taking into consideration the temperature distribution in the heat exchangers and at the battery, the vehicle speed, fan power and size. Moreover, the consideration of other atmosphere conditions is a must. It is also suggested to do a time dependent analysis.

6. ACKNOWLEDGEMENTS

The authors would like to thank CAPES for the financial support. This research was based upon a R&D Project from ANEEL - National Agency – PD.0394-1910/2019, supported by Eletrobras Furnas e Serra do Facão Energia, with AVL cooperation.

7. REFERENCES

Bahman, A.M. and Groll, E.A., 2020. "Application of second-law analysis for the environmental control unit at high ambient temperature". *Energies*, Vol. 13, p. 3274.

Buysse, C. and Miller, J., 2021. "Transport could burn up the eu's entire carbon budget". The International Council on Clean Transportation, https://theicct.org/blog/staff/eu-carbon-budget-apr2021. Accessed 28 june 2021.

dos Santos, E.O., 2005. *Dimensionamento e avaliação do ciclo de refrigeração de sistema de climatização automotivo*. Master's thesis, Graduate Program in Automotive Engineering, University of São Paulo, São Paulo, Brazil.

IEA, 2019. "Global ev outlook 2019: Scaling-up the transition to electric mobility". Internation Energy Agency.

Incropera, F., DeWitt, D.P., Bergman, T.L. and Lavine, A.S., 2006. *Fundamentals of Heat and Mass Transfer*, Vol. 6. John Wiley & Sons, New York.

Kim, J., Oh, J. and Lee, H., 2019. "Review on battery thermal management system for electric vehicles". *Applied Thermal Engineering*, Vol. 149, pp. 192–212.

Klein, S.A., 2016. "EES – engineering equation solver". Version 10.166 (2016-11-20). F-Chart Software.

Musser, A., Hrnjak, P. and Elbel, S., 2016. "Internal heat exchanger performance quantification and comparison testing methods including exploration of the effects of location of measurements and oil in circulation". In *Proceedings of the International Refrigeration and Air Conditioning Conference*.

Pham, H.M. and Rajendran, R., 2012. "R32 and hfos as low-gwp refrigerants for air conditioning". In *Proceedings of the International Refrigeration and Air Conditioning Conference*.

Simões-Moreira, J.R. and Neto, A.H., 2019. *Fundamentos e aplicações da psicrometria*, Vol. 2. Blucher, São Paulo.

Wickramaratne, L.S., 2017. *Battery thermal management system (Formula Student)*. Master's thesis, Graduate Program in Mechanical Engineering, University of Wolverhampton, Wolverhampton, United Kingdom.

8. RESPONSIBILITY NOTICE

The authors are solely responsible for the printed material included in this paper.